PCCP

RSC Publishing

PAPER

View Article Online
View Journal | View Issue

Temperature effects in dye-sensitized solar cells†

Cite this: *Phys. Chem. Chem. Phys.*, 2013, **15**, 2328

Sonia R. Raga and Francisco Fabregat-Santiago*

Received 13th September 2012,
Accepted 10th December 2012

DOI: 10.1039/c2cp43220j

www.rsc.org/pccp

In the standard solar cell technologies such as crystalline silicon and cadmium telluride, increments of temperature in the cell produce large variations in the energy conversion efficiency, which decreases at a constant rate. In dye solar cells the efficiency remains roughly constant with a maximum at around 30–40 °C and further decays above this temperature. In this work, the origin of this characteristic behavior is explained. Data show that under illumination recombination kinetics in the active layer of the cell is the same between −7 and 40 °C. Consequently, the efficiency of the cell remained virtually constant, with only small differences in the fill factor associated with changes in the series resistance. A further increase in temperature up to 70 °C produces an increase in recombination kinetics yielding lower photopotential and device performance. Finally, it is emphasized that at the normal operating temperatures of solar cells, the gap among the conversion efficiency of different technologies is much smaller than generally acknowledged.

Introduction

Dye sensitized solar cells (DSCs) are a promising alternative to silicon or thin film solar cells due to the low cost materials and simplicity in their fabrication process. These characteristics make DSC technology a candidate for large scale production of cheap energy.[1,2] The highest efficiencies reached with DSCs, 11–12%,[3–6] have been obtained using TiO_2 nanostructures for collecting the electrons, a redox electrolyte based on I^-/I_3^- for transporting the holes and a ruthenium dye attached to the semiconductor nanoparticles for absorbing the radiation and separating the charges into the different charge carrier media.[7,8] A recent publication has also reported 12% efficiency with porphyrin dyes and cobalt based redox electrolyte.[9]

Some of the beneficial characteristics of DSCs are that they maintain a high efficiency under diffuse or low light incident angle and that their performance presents little changes at environmental temperatures ranging between −20 and 80 °C.[10–13] Power conversion efficiency drops for rising temperatures in the case of the most extended technologies, at rates around −0.45% K^{-1} in mono- and polycrystalline silicon cells and of −0.25% K^{-1} for cadmium telluride.[14] In normal operation, cell temperatures (NOCT) rise to about 45–50 °C and consequently, their efficiency drops from nominal values approximately 10% for Si and 5% for CdTe. Dye solar cells instead present a maximum in the energy conversion efficiency close to NOCT.[12] This is a key aspect in the discussion of best performing solar cell technologies: as DSCs for 17 cm^2 modules have reached 9.9% efficiency,[15] the increase in efficiency at NOCT together with the decrease in the other technologies reduces the efficiency gap under the real operating conditions to a short distance.

From a more fundamental view, the progress in the field of DSCs has been very exciting in the last few years from both points of view, the enhancement of the device performance and the development of the models needed to understand the origin of the behavior of DSCs. Very relevant contributions have been focused on describing the mechanisms that control parameters such as the short circuit photocurrent, J_{sc}, open circuit photopotential, V_{oc}, and fill factor, FF, that determine the performance of the solar device.[16–19]

In general, charge collection is well resolved in DSCs, with efficiencies close to 100% in good cells. Photovoltage, however, presents large variations affected by charge recombination between TiO_2, dye or electrolyte composition and also by the energetic position of the TiO_2 conduction band in relation to the redox energy level in the electrolyte.[20–22] Recombination of charge plays a major role in the photopotential attained by the DSC[17,22] and it is determined by different mechanisms that involve variations in acceptor species: Miyashita *et al.*[23] proposed that there is a locally increased concentration of I_3^- near the dye under illumination and Boschloo and Hagfeldt[16] remarked the generation of other acceptor species as $I_2^{-\bullet}$. On another hand O'Regan and Durrant[24] suggested that recombination increases

Photovoltaic and Optoelectronic Devices Group, Departament de Física, Universitat Jaume I, 12071 Castelló, Spain. E-mail: fran.fabregat@fca.uji.es; Fax: +34-964-729218; Tel: +34-964-387537

† Electronic supplementary information (ESI) available: Measures of performance of DSC for 500 h lifetime tests, Nyquist plots showing series resistances, values of conduction band shifts, plots of capacitance values *vs.* V_{ecb}, comparison of capacitance in the dark and under illumination, comments on transport resistance and performance data of DSC after shifting the applied potential the displacement in the conduction band edge (ΔE_c). See DOI: 10.1039/c2cp43220j

due to a binding between dye molecules and iodine, an effect that does not exclude the previously mentioned ones. Moreover, recombination of charge increases when the TiO_2 conduction band position decreases.[25,26]

In this paper we used previously developed models to report the effect of temperature on DSCs. To simplify the analysis, we focused the study on the FF and V_{oc} while keeping the short circuit photocurrent constant. Current density *vs.* potential (*J–V*) curves and impedance spectroscopy (IS) measurements were taken both in the dark and under illumination in a temperature range between −7 °C and 70 °C. A detailed analysis of the origin of the characteristic behavior of the parameters governing the performance of the solar cells is provided and an explanation for the changes in the energy conversion efficiency with the temperature is given.

Experimental

Dye-sensitized solar cell preparation

Working electrodes for the DSC were prepared on 2.3 mm thickness and 15 Ω $\square^{-1}$ FTO glass plates. First, glasses were brushed with detergent solution and rinsed with Milli-Q water, then immersed into iso-propanol and cleaned using an ultrasonic bath for 15 min, then rinsed with ethanol and dried with air. After that a 150 nm compact TiO_2 layer was deposited by the spray-pyrolysis technique with an ethanol/acetyl acetone/titanium(IV) isopropoxide (3 : 3 : 2 weight ratio) solution and a 450 °C hot plate. The substrates were coated by the doctor blade technique with a 7 μm layer of 20 nm size TiO_2 nanoparticles and a 3 μm scatter layer of 450 nm size TiO_2 nanoparticles (respectively 18-NRT and WER4-0 from Dyesol), then fired 30 min at 450 °C. The active area of the film was 0.25 cm^2. When cooled, films were immersed into 40 mM $TiCl_4$ (aq) at 70 °C for 30 min, rinsed with Milli-Q water and sintered at 570 °C for 10 min. After cooling to 40 °C, the TiO_2 electrodes were immersed into a N719 dye solution (0.5 mM in a mixture of acetonitrile and *tert*-butanol, 1 : 1 volume ratio) for 16 hours.

As counter electrodes, 8 Ω $\square^{-1}$ FTO coated glasses were drilled with a 1 mm diameter drill tip and cleaned with the same procedure as mentioned above. The counter electrodes were prepared with a drop of chloroplatinic acid solution from Sigma Aldrich on the FTO and then fired in a 450 °C air flow.

The working and counter electrodes were assembled in a sandwich-type cell by pressing at 95 °C with a hot-melt film (Surlyn 25 μm thickness) as a sealant and spacer between electrodes. A drop of electrolyte solution (0.60 M 1-butyl-3-methylimidazolium iodide, 0.03 M I_2, 0.10 M guanidinium thiocyanate, and 0.50 M 4-*tert*-butylpyridine in methoxypropionitrile) was placed on the drilled holes, then the cell was placed into a small chamber where vacuum was applied until most of the air inside the cell bubbled out through the electrolyte, when air came again into the chamber the electrolyte was driven into the cell. Finally the drilled holes were sealed with Surlyn and 0.1 mm thick glasses, and a tin contact was welded on the edge of FTO outside the cells. Five cells were prepared for statistical significance and a 500 h stability test was performed. Average performance data under 1 sun AM1.5G illumination at room temperature are provided in Fig. S1 of ESI.† The average performance evolution with time is shown in Fig. S2 (ESI†). The most stable cells were chosen for the study of impedance.

Solar cell characterization

J–V curves were taken using a Keithley 2612 System Source Meter. Impedance measurements were carried out using a FRA-equipped PGSTAT-30 from Metrohm-Autolab, applying a 25 mV AC signal at low potentials and a 10 mV AC signal at high potentials, we could minimize the noise while keeping linearity in the response of the DSC. The frequency of the measurements was scanned between 400 kHz and 0.1 Hz at forward applied bias that ranged from 0.3 V to 0.9 V. Below 0.3 V the large impedance found corresponds to FTO and impedance data are not needed for the interpretation of DSC behavior.

At environmental temperature, for fresh samples and during the ageing experiments shown in ESI,† illumination was provided by a solar simulator filtered at AM1.5G and light intensity adjusted with an NREL-calibrated Si solar cell with a KG-5 filter to 1 sun intensity (100 mW cm^{-2}). A white-light LED lamp was used to obtain *J–V* curves and impedance spectroscopy measurements in temperature controlled experiments. The power of the LED lamp was adjusted (with variations < 2%) to obtain the same photocurrent as that provided with the 1 sun AM1.5G solar simulator at environmental temperature. Proceeding this way is important for several reasons: analysis of data at the same current makes it much clear to state the gross effects of temperature in the solar cell; the absence of IR light in the LED lamp ensures a minimum influence of the power source in the temperature of the device; finally, temperature variations have little effects in short circuit current. Together with the fact that the small changes in illumination intensity to keep the current constant produce tiny variations in V_{oc} and FF, this ensures that changes in efficiency are minimal. However, as the light spectrum is not matching AM1.5G standard and the illumination power is not exactly the same in all the measurements, we used the term apparent efficiency instead of efficiency to describe DSC performance.

The temperature was controlled using a Peltier cell monitored by a computer, in the range of temperatures from −7 °C to 70 °C. Note that for allowing the better illumination possible, the counter electrode side of the DSC is in contact with the refrigerating Peltier element.

Results and discussion

Fig. 1 shows the effect of temperature on the *J–V* curves of a DSC taken both in the dark and under LED illumination equivalent to 1 sun. In Fig. 1(a), it may be observed that the rise in temperature produces an onset of photocurrent at lower potentials and thus under illumination (Fig. 1(b)) this shift is translated into a decrease in open circuit voltage.

For a better understanding of the origin of this behavior, we have examined the physical processes occurring in DSCs by means of IS, carried out at each of the measured temperatures. Characteristic Nyquist plots are shown in Fig. S3 and S4 of ESI.†

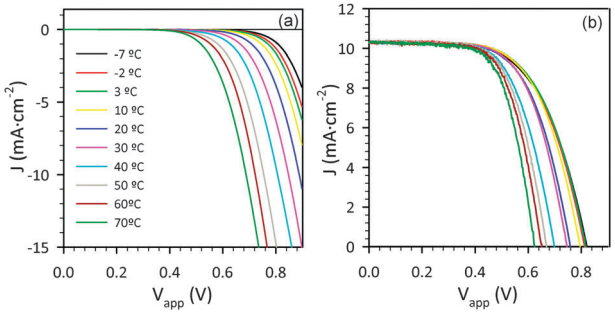

Fig. 1 *J–V* curves at different temperatures obtained after IS measurements in the dark (a) and under illumination (b) conditions.

The analysis of impedance spectra has been made by employing the equivalent circuits previously reported for DSCs.[25] This allows studying separately parameters, such as the chemical capacitance (C_μ) and the recombination (R_{rec}) and transport resistances (R_{tr}), that describe the processes of accumulation, loss and transport of the charge in the TiO_2 and the different contributions to total series resistance given by

$$R_{series} = R_{FTO} + R_{Pt} + R_d \quad (1)$$

with R_{FTO} the resistance of the conducting glass plus contacts and wires, R_{Pt} the charge transfer resistance at the platinized counter electrode and R_d the diffusion resistance originated by the transport of holes in the electrolyte.

We focus first on the effect of temperature over R_{series}. Fig. 2 shows the average values of the different contributions to R_{series}. At high temperatures, the main contributor to R_{series} is R_{FTO} which presents a nearly constant value for all the temperatures both in the dark and under illumination, Fig. 2(a). This result is confirmed by measurements of plain FTO in which the same trend, a very slight increase in R_{FTO} with rising temperature, is observed, see Fig. 3(a). Note that while cell design may reduce R_{FTO}, once it is established, temperature has little effect on it.

At low temperatures, as may be seen in Fig. 2(b) and (c), charge transfer at the counter electrode and diffusion resistance in the electrolyte showed comparable or even larger values than R_{FTO}. In Fig. 2(b) it may be observed that R_{Pt} in the dark and under illumination presents the same values, which rise as the temperature diminishes. This result indicates that the counter electrode is in thermal equilibrium with the cooling plate over which it is located. The reduction in R_{Pt}, with rising temperatures, is attributed to the acceleration of charge transfer kinetics with the redox regeneration.

Diffusion resistance of the electrolyte shown in Fig. 2(c) presents both variations under illumination conditions and external temperature of the cell. At high temperatures decrease in the electrolyte resistance is expected under illumination as the increased concentration of I_3^- due to the regeneration of the dye increases the conductivity in the solution. However this change seems not enough to explain the large differences found for R_d at low external temperatures. In the dark, the increase in R_d indicates an increment in the viscosity of the electrolyte when temperature diminishes.[27] Under illumination, part of the electrolyte is in contact and in thermal equilibrium with the TiO_2 film which could present a higher temperature than that of the counter electrode. Therefore, a gradient of temperature will be built in the electrolyte between these two electrodes. This gradient could be remarkable as the distances between the hot active electrode and the cold counter electrode are constrained to 15 μm. Under these conditions electrical measurements provide a value of R_d associated with the average viscosity of the electrolyte.

In summary, total series resistance decreases with rising temperatures due to the changes in R_{Pt} and R_d, while R_{FTO} remains nearly constant. The first two resistances dominate at low temperatures while the last one provides the main R_{series} contribution at high temperature.

For an accurate analysis of the parameters associated with TiO_2, applied potential needs to be corrected from the potential drop at R_{series} at each temperature. As may be observed in Fig. 3(b) and (c), R_{Pt} and R_d change also with potential, therefore to obtain the potential drop at the TiO_2 film, $V_F = (E_{Fn} - E_{F0})/q$, it is needed to proceed through the integral[17,29]

$$V_F = V_{app} + \frac{J}{J_{sc} - J}\int_{J_{sc}}^{J} R_{series} dJ \quad (2)$$

Fig. 4 shows the chemical capacitance of the TiO_2. Measurements of C_μ in the dark and under illumination, Fig. 4(a) and (b), show very similar slopes at high potentials, following the expression[28]

$$C_\mu = C_0 \exp\left[\frac{q}{k_B T_0} V_F\right] \quad (3)$$

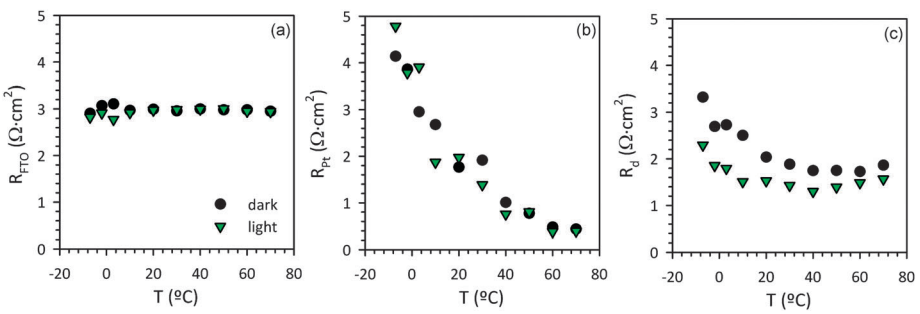

Fig. 2 Temperature dependence of the different contributions to the series resistance of the DSC. (a) Resistance of the FTO conducting glass plus contacts and wires; (b) resistance of the platinized counter electrode; and (c) diffusion resistance.

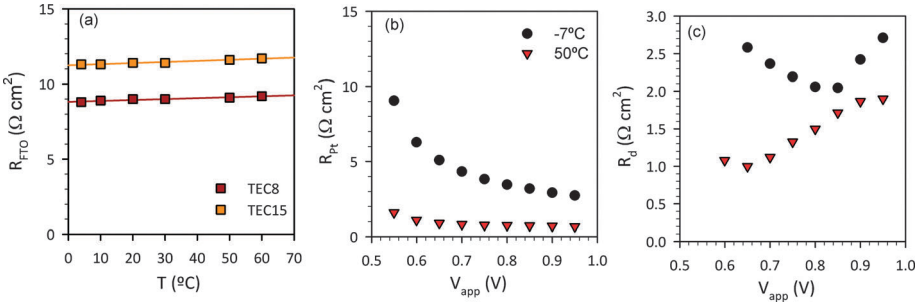

Fig. 3 (a) Changes in the resistance of two 1 cm^2 FTO samples with temperature. As for our samples their change is minimal with a slight increase with rising temperatures. Changes with applied potential are lower than 5%. The effect of potential is relevant both for counter electrode resistance (b) and diffusion resistance (c). At low temperatures these resistances take larger values than at high temperatures. The minimum in R_d in (c) occurs near V_{oc} where current crossing the cell is zero. Note that the overlap between recombination and diffusion arc shown in Fig. S3 and S4 (ESI†) produces increasing errors (>20%) in the values of R_d at the lower potentials.

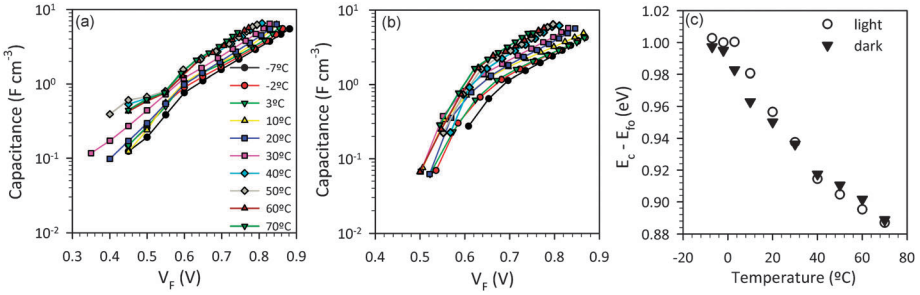

Fig. 4 Values of TiO_2 capacitances: (a) in the dark and (b) under illumination conditions. (c) Values of conduction band position during the measurements.

where T is the film temperature, q the electron charge, k_B the Boltzmann constant, T_0 a parameter with temperature units determining the depth of the trap distribution tail under conduction band, and C_0 a parameter given by

$$C_0 = \frac{(1-p)Lq^2N_L}{k_BT_0}\exp\left[\frac{q}{k_BT_0}(E_{F0}-E_c)\right] \qquad (4)$$

where p is the porosity of the TiO_2 layer, L the thickness, N_L the total electron trap density,[30,31] $E_{F0} - E_c$ is the difference between the dark (equilibrium) Fermi level and conduction band position of TiO_2.

In previous studies, it has been shown that chemical capacitance is independent of temperature.[4,32] However, if nanoparticles are small enough, the series contribution of Helmholtz capacitance may produce visible effects on the total capacitance of the film.[33,34] Here we find that C_μ values are clearly shifted towards lower potentials for increasing temperatures. Although this displacement would agree with changes in the Helmholtz capacitance with temperature, the relatively large displacement of the capacitance and the constant slope *vs.* the potential are not compatible with an explanation based on Helmholtz contribution.[29]

Other possible origin of the shift in C_μ could be on changes in the E_{redox} (E_{F0}) due to temperature. The Nernst equation has been used to calculate the change in E_{redox} yielding a change lower than 10 mV in the full range of temperatures. Assuming that neither the distribution nor the total amount of trap states changed with temperature, we may attribute the shift observed in C_μ to a displacement in the energy of the conduction band.[35]

Eqn (4) was used to estimate the E_c position for each temperature using $N_L = 2.5 \times 10^{19}$ cm^{-3}. Fig. 4(c) shows the reduction in the E_c level during measurements which, within the experimental error, was nearly the same both in the dark and under illumination conditions. Transport resistance was also used to test changes in E_c yielding the same conclusions, see ESI† for more details.

Movement of the position of the E_c during aging of cells is a phenomenon well known by experimentalists in the field. It depends on time and also on measurement conditions, which produces a variety of behaviors: sometimes E_c rises with time,[36] commonly in fresh samples, in other occasions it drops.[37] In our case, the cells were pre-aged for 500 h (see Fig. S1 in ESI†) before the IS measurements to increase stability and reproducibility of data. Repeated measurements at 20 °C after completing the measurement of the temperature series yielded the same E_c value obtained for TiO_2 at this temperature during the series measurement. This result suggests reversibility in TiO_2 E_c movement with temperature that, as far as we know, is reported for the first time. The origin of this behavior of E_c with temperature found for our samples is not yet clear. One possibility could be reversible adsorption/desorption of electrolyte additives, dye or even environmental contamination (*i.e.* H^+ from H_2O) at the surface of the TiO_2. Other possibility could be narrowing of band gap of TiO_2 with temperature. Future work should be devoted to clarify this aspect.

To analyze separately the effects of the variations in E_c in the performance of the DSC from other contributions, the voltage needs to be corrected from the conduction band shift at the

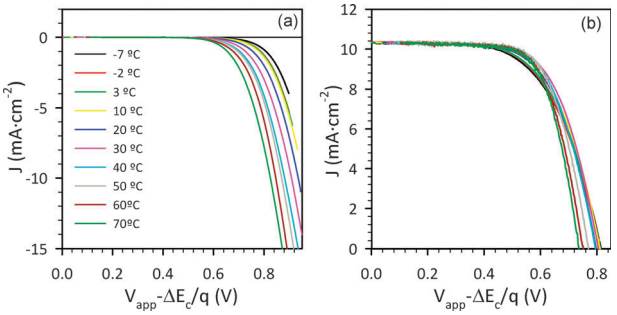

Fig. 5 *J–V* curves from Fig. 1 after shifting the applied potential by the difference in the conduction band energy with respect to the measurements taken at 50 °C. (a) In the dark and (b) under illumination.

different temperatures,[20] so we used $\Delta E_c(T) = E_c(T) - E_c(-7\ ^\circ\mathrm{C})$ with −7 °C (dark) as the reference temperature for comparison. Data are summarized in Table S1 of ESI.†

Fig. 5 shows the modified *J–V* curves obtained after addition of ΔE_c to the voltage. In the dark, Fig. 5(a), the onset in photocurrent occurs at lower voltages with increasing temperature however, under illumination, Fig. 5(b), V_{oc} takes the same values for all curves up to 40 °C. Only the measurements above 50 °C present a noticeable decrease in V_{oc}. This result indicates that in the dark a rise in the temperature of the sample produces an increase in recombination rate, while for illuminated samples up to 40 °C this effect does not occur. Therefore, the changes in V_{oc} up to 40 °C are only produced by E_c shifts and not due to changes in charge transfer rate associated with temperature.

To explain this result we focus now on the analysis of the recombination resistance. As published before, once the short circuit photocurrent is fixed, V_{oc} and the ideal J–V_F curve (the J–V with $R_{series} = 0$) are determined by recombination kinetics that may be analyzed through the recombination resistance.[17,38,39] As

$$R_{rec} = \left(\frac{dJ}{dV_F}\right)^{-1}, \quad (5)$$

the photopotential is determined by

$$V_{oc} = V_0 + \int_{J_{sc}}^{0} R_{rec} dJ \quad (6)$$

and the current density at the different V_F by

$$J = J_{sc} - \int_{V_0}^{V_F} \frac{dV_F}{R_{rec}} \quad (7)$$

with V_0 the potential drop in series resistance of the cell under short circuit conditions.

According to eqn (6) and (7) the larger R_{rec} produces a smaller current density for a given potential for measurements taken in the dark ($J_{sc} = 0$ and $V_0 = 0$), while under illumination it yields a larger photopotential. Therefore the study of R_{rec} helps in the understanding of the obtained *J–V* curves.

Fig. 6(a) and (b) show the variation in recombination resistance *vs.* the corrected potential at the different temperatures measured both in the dark and under illumination. R_{rec} roughly follows

$$R_{rec} = R_0 \exp\left[-\frac{\beta q}{k_B T} V_F\right] \quad (8)$$

with β a coefficient associated with the non-linearity of the charge transfer process and equivalent to the non-ideality factor ($m = 1/\beta$) of the diode equation used for standard semiconductor solar cells, and R_0 the pre-exponential parameter.

This result agrees well with a recombination process occurring through extended surface states in an energy tail distributed below the CB which, following the probabilistic model of Marcus[40], after some simplifications yields eqn (8) with[32]

$$R_0 = \frac{T_0\sqrt{\pi\lambda k T}}{q^2 L k_0 c_{ox} N_s T} \exp\left[\frac{E_c - E_{redox}}{k_B T_0} + \frac{\lambda}{4 k_B T}\right] \quad (9)$$

where λ is the reorganization energy, L the film thickness, c_{ox} the concentration of acceptor species in the electrolyte, N_s the density of states near the TiO_2 surface and k_0 a time constant for tunneling, also named rate constant. Other contributions from recombination through localized surface states below the conduction band may also occur, which would modify eqn (8).[32]

The decrease in recombination resistance with increasing temperature shown in Fig. 6(a) and (b) is associated with a decrease in R_0 and is responsible for the onset of current loss that occurs at lower potentials, as the application of eqn (7) describes.[17] This fact explains the result of dark *J–V* curves shown in Fig. 1(a), and the decrease in the open circuit potential shown in Fig. 1(b) and Table 1.

Eqn (9) shows the dependence of R_0 on temperature, the concentration of acceptor species in the electrolyte and E_c. Therefore, the decrease in recombination resistance when increasing temperature shown in Fig. 6(a) and (b) should be also affected by the shift in E_c. If the definition of the common equivalent conduction band potential,[17,38,39]

$$V_{ecb} = V_F - \Delta E_c/q \quad (10)$$

is used, the representation of the recombination resistance *vs.* V_{ecb} provided in Fig. 6(c) and (d) allows the analysis of the data independently of E_c changes.

Thus under dark conditions, as can be seen in Fig. 6(c), R_{rec} decreases when temperature increases. This is the expected behavior attributed to an accelerated reaction kinetics of electrolyte acceptor species on the semiconductor surface due to the rising temperature.[32]

However, under illumination all the values of R_{rec} taken for temperatures equal and lower than 40 °C converge, see Fig. 6(d), and they have very close values to those of R_{rec} in the dark at 40 °C, see blue line in Fig. 6(d).

This phenomenon may have two origins: on the one hand and despite the cooling provided, the real temperature of the TiO_2 layer was increased to a value close to 40 °C for all the measurements done up to this temperature. This would imply that the heat accumulated into the active film due to the light

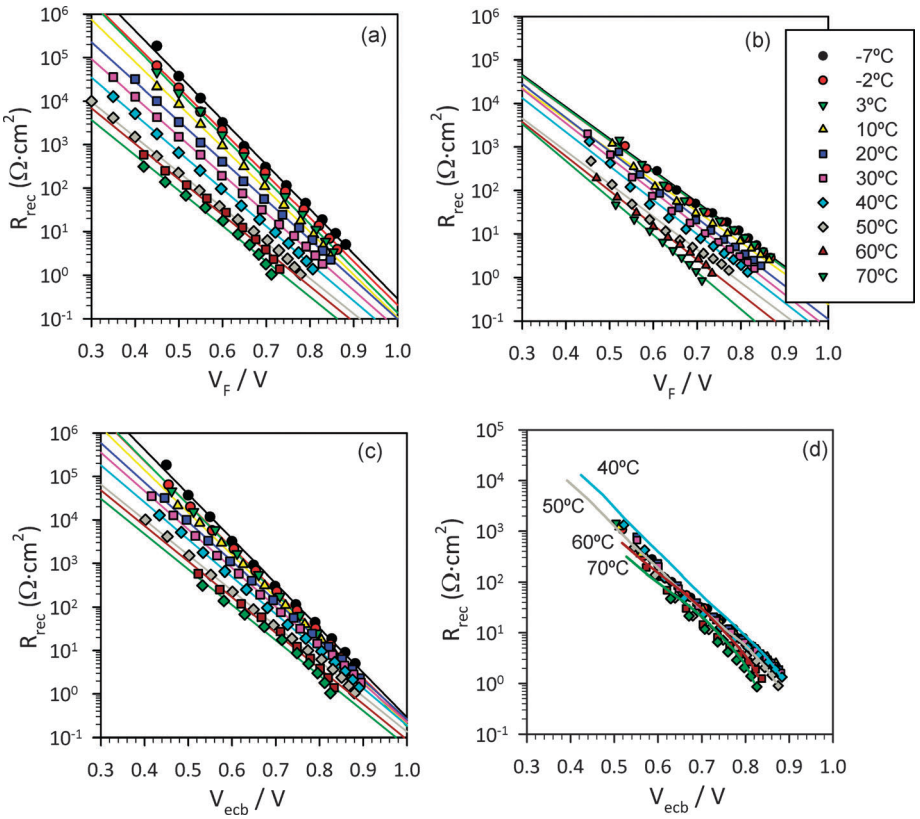

Fig. 6 Values of TiO_2 recombination resistances *versus* corrected potential in the dark (a) and under illumination conditions (b) and *versus* the equivalent conduction band potential in the dark (c) and under illumination (d). Lines in (d) represent R_{rec} under dark conditions for 40 °C (light blue), 50 °C (grey), 60 °C (brown) and 70 °C (dark green).

Table 1 Characteristic parameters determining the efficiency of DSCs and average series resistance in the range of temperatures indicated

T (°C)	J_{sc} (mA cm^{-2})	V_{oc} (V)	Fill factor	η_{app} (%)	R_{series} (Ω cm^2)
−7	10.3	0.82	0.60	5.10	9.9
−2	10.3	0.81	0.61	5.14	8.6
3	10.3	0.82	0.61	5.19	8.5
10	10.3	0.80	0.63	5.16	6.8
20	10.3	0.76	0.63	4.95	6.5
30	10.3	0.75	0.64	4.95	5.8
40	10.3	0.72	0.64	4.74	5.9
50	10.3	0.67	0.65	4.49	5.5
60	10.3	0.65	0.66	4.44	5.3
70	10.3	0.62	0.67	4.31	5.2

absorption from a high intensity irradiation source cannot be efficiently evacuated neither through the 2.3 mm thick FTO glass substrate nor through the electrolyte side. Note that despite the use of LED to illuminate the samples effects such as thermalization of charges and energy loss due to recombination and transport (Joule effect) still occur and would be responsible for the heating of the TiO_2 film.

A second possibility could be that the increased concentration of acceptor species in the electrolyte (*i.e.* I_3^-) close to the TiO_2 surface after dye regeneration would increase the recombination to levels close to those occurring at 40 °C in the dark.

In our case, the precision obtained for transport resistance data, see ESI,† is not enough to discriminate which of the two phenomena is dominating. The shift in the conduction band with rising temperatures shown in Fig. 4(c) suggests that the second phenomenon dominates, but a local increase in film temperature cannot be fully discarded.

As shown in Fig. 6(d), for the measurements taken above 50 °C under illumination, R_{rec} is smaller than at 40 °C, in a similar manner than for dark measurements, which may be attributed to a faster recombination kinetics attained at these higher temperatures. The effect of this reduction in R_{rec} is that for temperatures larger than 50 °C, the photopotential decreases with respect to the other temperatures as shown in Fig. 5(b).

In Fig. 6(d) it is possible to observe small differences between R_{rec} in the dark and under illumination. This implies that recombination in the illuminated sample is a more complex process than the single mechanism provided by eqn (8). Other contributions to recombination processes may be related to variations in acceptor species in the electrolyte. A more detailed study about this aspect and how it modifies eqn (8) is out of the scope of this paper and will be analyzed in a separate piece of work.

The result of the combination of the behavior of recombination and series resistances produces the characteristic shape of DSCs, the efficiency temperature curve is shown in Fig. 7. Our data, taken from J–V_{app} curves after ΔE_c correction (see Fig. 5(b) and Table S2 in ESI†), have been normalized to be able to

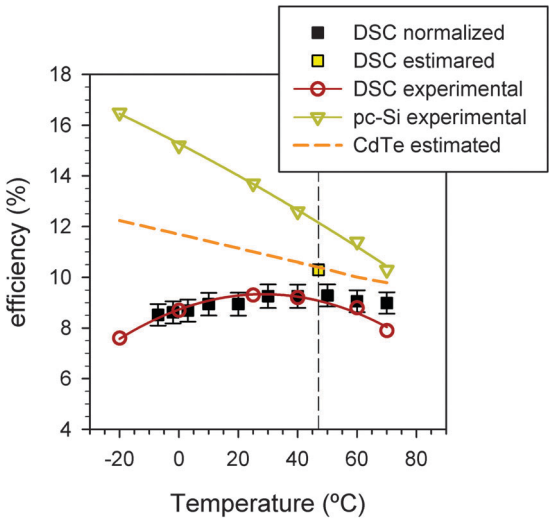

Fig. 7 Comparison of energy conversion efficiencies for different photovoltaic technologies and temperatures. Black squares represent the apparent efficiency obtained from *J–V* curves in Fig. 5(b) normalized to match the published data of a 9.3% efficient DSC module (red void circles). Error bars are included to represent the mismatch with standard AM1.5G illumination conditions. Yellow square represents the estimation obtained for the record 9.9% efficient module taking into consideration extra energy collected by DSCs under real outdoor conditions. pc-Si experimental (green triangles) stands for data from a commercial polycrystalline silicon solar module and CdTe estimated (orange dashed line) is the simulation of a 11% module with a temperature coefficient of $-0.25\%\ K^{-1}$. The dotted line represents the NOCT temperature, where performance comparison approaches real operation conditions.

compare the results with data published from Sony for a 9.3% efficient DSC 17 cm^2 module.[12] The good match found suggests similar mechanisms dominating the behavior of both cell and module.

Therefore at low temperatures while recombination rate in the TiO_2 film is constant, the decrease in the counter and diffusion contributions to the total series resistance of the DSC with increasing temperatures improves FF. Between 20 and 40 °C both R_{rec} and R_{series} present little changes and so does efficiency. Above 40 °C the decrease in recombination resistance and thus the V_{oc} produces a reduction in the efficiency that may not be compensated by further increases in FF. For these temperatures, see Fig. 2, R_{series} is dominated by the nearly constant R_{FTO}, while R_d stabilizes and R_{Pt} presents only a small reduction.

As mentioned above, the fact that the maximum efficiency in a DSC is obtained at a temperature close to the normal operating cell temperature (NOCT) is an aspect to take into account when comparing DSCs with other technologies. Therefore, considering 47 °C as NOCT, the efficiency of a CdTe module drops from a nominal value of 11% to a practical value of 10.4% while a polycrystalline silicon (pc-Si) module with a nominal efficiency of 13.7% presents, at this NOCT, a real efficiency of 12.3%, see Fig. 7.

Record DSC modules reaching 9.9% efficiency are not so far from the values obtained for these standard and commercial panels.[15] Furthermore, the ability of DSCs to capture low incidence angle and diffuse light results in both an extension of effective energy production hours and a higher performance in cloudy days.[10,13] Energy production increases of 10% in sunny days and 20% in cloudy days have been reported for DSCs with respect to pc-Si modules for outdoor static installations with the same nominal power.[10,13] Part of this rise in energy output is due to the lower real efficiency of pc-Si at NOCT, as just mentioned. Therefore, considering a rough 5% as the "effective" performance increase in the DSC per watt peak installed with respect to conventional technologies, the comparable efficiency of the DSC would rise to 10.3% for a nominal 9.9% module, see yellow square in Fig. 7. This is at the same level than CdTe panels at NOCT.

Conclusions

We have observed that out of conduction band shifts, electron loss by recombination in TiO_2 is the same for external temperatures ranging between −7 and 40 °C. This effect may be due to the combined effect of a rise in the temperature of active film and the increase in the acceptor species in the electrolyte close to the TiO_2 surface after dye regeneration under high light intensity. The constant recombination resistance pattern in this range of temperatures determines the constant V_{oc} attained for data compared at the same position of conduction band. The decrease in total series resistance with rising temperatures produces an increase in FF and thus in efficiency up to this high temperature. Above 40 °C recombination accelerates producing a decay in V_{oc}. As further reduction in series resistance is limited, efficiency decreases above 40 °C are observed.

Finally we remarked that for a correct comparison of efficiencies between solar technologies the values at operating temperatures should be used rather than the nominal ones. This yields a narrower and more realistic gap between the different technologies than under nominal conditions.

Acknowledgements

Financial support from Ministerio de Cíencia e Innovación under project HOPE CSD2007-00007 and Generalitat Valenciana under Project PROMETEO/2009/058 are acknowledged. Serveis Centrals d'Instrumentació Científica from Universitat Jaume I are acknowledged for the profilometry measurements. SRR thanks Pablo P. Boix for helping in lab setup.

References

1 M. Grätzel, Dye-sensitized solar cells, *J. Photochem. Photobiol., C*, 2003, **4**, 145–153.
2 V. Marin, E. Holder, M. M. Wienk, E. Tekin and D. Kozodaev, Schubert, U. S. Ink-Jet Printing of Electron Donor/Acceptor Blends: Towards Bulk Heterojunction Solar Cells, *Macromol. Rapid Commun.*, 2005, **26**, 319–324.
3 Y. Chiba, A. Islam, Y. Watanabe, R. Komiya, N. Koide and L. Han, Dye-Sensitized Solar Cells with Conversion Efficiency of 11.1, *Jpn. J. Appl. Phys.*, 2006, **45**, L638–L640.

4 Y. Cao, Y. Bai, Q. Yu, Y. Cheng, S. Liu, D. Shi, F. Gao and P. Wang, Dye-Sensitized Solar Cells with a High Absorptivity Ruthenium Sensitizer Featuring a 2-(Hexylthio)thiophene Conjugated Bipyridine, *J. Phys. Chem. C*, 2009, **113**, 6290–6297.

5 Q. Yu, Y. Wang, Z. Yi, N. Zu, J. Zhang, M. Zhang and P. Wang, High-Efficiency Dye-Sensitized Solar Cells: The Influence of Lithium Ions on Exciton Dissociation, Charge Recombination, and Surface States, *ACS Nano*, 2010, **4**, 6032–6038.

6 M. Grätzel, *Hybrid and Organic Photovoltaic Conference, HOPV'11*, 2011, Valencia, Spain.

7 B. C. O'Regan and M. Grätzel, A low-cost high-efficiency solar cell based on dye-sensitized colloidal TiO_2 films, *Nature*, 1991, **353**, 737.

8 M. K. Nazeeruddin, A. Kay, I. Rodicio, R. Humphry-Baker, E. Müller, P. Liska, N. Vlachopoulos and M. Grätzel, Conversion of light to electricity by *cis*-X 2bis(2,2′-bipyridyl-4,4′-dicarboxylate)ruthenium(II) charge-transfer sensitizers (X = Cl^-, Br^-, I^-, CN^-, and SCN^-) on nanocrystalline TiO_2 electrodes, *J. Am. Chem. Soc.*, 1993, **115**, 6382–6390.

9 A. Yella, H.-W. Lee, H. N. Tsao, C. Yi, A. K. Chandiran, M. K. Nazeeruddin, E. W.-G. Diau, C.-Y. Yeh, S. M. Zakeeruddin and M. Grätzel, Porphyrin-Sensitized Solar Cells with Cobalt(II/III) Based Redox Electrolyte Exceed 12 Percent Efficiency, *Science*, 2011, **334**, 629–634.

10 T. Toyoda, T. Sano, J. Nakajima, S. Doi, S. Fukumotoa, A. Ito, T. Tohyamaa, M. Yoshida, T. Kanagawa, T. Motohiro, T. Shiga, K. Higuchi, H. Tanaka, Y. Takeda, T. Fukano, N. Katoh, A. Takeichi, K. Takechi and M. Shiozawa, Outdoor performance of large scale DSC modules, *J. Photochem. Photobiol., A*, 2004, **164**, 203–207.

11 K. Kalyanasundaram, Dye-sensitized Solar Cells, in *Dye-sensitized Solar Cells*, ed. K. Kalyanasundaram, CRC Press, Boca Raton, 2010.

12 T. Nozawa, Organic Solar Cells Now Produced in Volume. *Nikkei Electronics Asia* 2008, *July*, http://techon.nikkeibp.co.jp/article/HONSHI/20080625/20153868/.

13 K. Brooks, P. Murray, F. Au, H. Duong, R. Harikisun, H. Desilvestro, Status of Industrialization of Dye Solar Cells for BIPV Applications. In 3rd Nordic PV Conference Tallinn, Estonia, 2009, Vol. http://www.irc.ee/pvconference/?page=participants.

14 H.-D. Mohring, D. Stellbogen, ''Annual Energy Harvest of PV Systems – Advantages and Drawbacks of Different PV Technologies.'', 23rd European Photovoltaic Solar Energy Conference, 1–5 September 2008, 2008, Valencia, Spain.

15 M. Morooka, R. Ogura, M. Orihashi and M. Takenaka, Development of dye-sensitized solar cells for practical applications, *Electrochemistry*, 2009, **77**, 960–965.

16 G. Boschloo and A. Hagfeldt, Characteristics of the Iodide/Triiodide Redox Mediator in Dye-Sensitized Solar Cells, *Acc. Chem. Res.*, 2009, **42**, 1819–1826.

17 F. Fabregat-Santiago, G. Garcia-Belmonte, I. Mora-Sero and J. Bisquert, Characterization of nanostructured hybrid and organic solar cells by impedance spectroscopy, *Phys. Chem. Chem. Phys.*, 2011, **13**, 9083–9118.

18 J. R. Jennings, Y. R. Liu and Q. Wang, Efficiency Limitations in Dye-Sensitized Solar Cells Caused by Inefficient Sensitizer Regeneration, *J. Phys. Chem. C*, 2011, **115**, 15109–15120.

19 J. Bisquert and F. Fabregat-Santiago, Impedance spectroscopy: A general introduction and application to dye-sensitized solar cells, in *Dye-sensitized Solar Cells*, ed. K. Kalyanasundaram, EPFL Press, CRC Press, Lausanne, Boca Raton, 2010.

20 Z. Zhang, P. Chen, T. N. Murakami, S. M. Zakeeruddin and M. Gratzel, The 2,2,6,6-tetramethyl-1-piperidinyloxy radical: An efficient, iodine-free redox mediator for dye-sensitized solar cells, *Adv. Funct. Mater.*, 2008, **18**, 341–346.

21 T. Daeneke, T.-H. Kwon, A. B. Holmes, N. W. Duffy, U. Bach and L. Spiccia, High-efficiency dye-sensitized solar cells with ferrocene-based electrolytes, *Nat. Chem.*, 2011, **3**, 211–215.

22 S. R. Raga, E. M. Barea and F. Fabregat-Santiago, Analysis of the Origin of Open Circuit Voltage in Dye Solar Cells, *J. Phys. Chem. Lett.*, 2012, **3**, 1629–1634.

23 M. Miyashita, K. Sunahara, T. Nishikawa, Y. Uemura, N. Koumura, K. Hara, A. Mori, T. Abe, E. Suzuki and S. Mori, Interfacial Electron-Transfer Kinetics in Metal-Free Organic Dye-Sensitized Solar Cells: Combined Effects of Molecular Structure of Dyes and Electrolytes, *J. Am. Chem. Soc.*, 2008, **130**, 17874–17881.

24 B. C. O'Regan and J. R. Durrant, Kinetic and Energetic Paradigms for Dye-Sensitized Solar Cells: Moving from the Ideal to the Real, *Acc. Chem. Res.*, 2009, **42**, 1799–1808.

25 F. Fabregat-Santiago, J. Bisquert, G. Garcia-Belmonte, G. Boschloo and A. Hagfeldt, Impedance spectroscopy study of the influence of electrolyte conditions in parameters of transport and recombination in dye-sensitized solar cells, *Sol. Energy Mater. Sol. Cells*, 2005, **87**, 117–131.

26 Y. Liu, A. Hagfeldt, X.-R. Xiao and S.-E. Lindquist, Investigation of influence of redox species on the interfacial energetics of a dye sensitized nanoporous TiO_2 solar cell, *Sol. Energy Mater. Sol. Cells*, 1998, **55**, 267–281.

27 F. Fabregat-Santiago, J. Bisquert, E. Palomares, L. Otero, D. Kuang, S. M. Zakeeruddin and M. Grätzel, Correlation between Photovoltaic Performance and Impedance Spectroscopy of Dye-Sensitized Solar Cells Based on Ionic Liquids, *J. Phys. Chem. C*, 2007, **111**, 6550–6560.

28 J. Bisquert, Chemical capacitance of nanostructured semiconductors: its origin and significance for heterogeneous solar cells, *Phys. Chem. Chem. Phys.*, 2003, **5**, 5360.

29 J. Bisquert, F. Fabregat-Santiago, I. Mora-Seró, G. Garcia-Belmonte and S. Giménez, Electron Lifetime in Dye-Sensitized Solar Cells: Theory and Interpretation of Measurements, *J. Phys. Chem. C*, 2009, **113**, 17278–17290.

30 G. Boschloo and D. Fitzmaurice, Spectroelectrochemical Investigation of Surface States in Nanostructured TiO_2 Electrodes, *J. Phys. Chem. B*, 1999, **103**, 2228–2231.

31 F. Fabregat-Santiago, I. Mora-Seró, G. Garcia-Belmonte and J. Bisquert, Cyclic voltammetry studies of nanoporous semiconductor electrodes. Models and application to nanocrystalline TiO_2 in aqueous electrolyte, *J. Phys. Chem. B*, 2003, **107**, 758–769.

32 Q. Wang, S. Ito, M. Grätzel, F. Fabregat-Santiago, I. Mora-Seró, J. Bisquert, T. Bessho and H. Imai, Characteristics of High Efficiency Dye-sensitized Solar Cells, *J. Phys. Chem. B*, 2006, **110**, 19406–19411.

33 I. Abayev, A. Zaban, V. G. Kytin, A. A. Danilin, G. Garcia-Belmonte and J. Bisquert, Properties of the electronic density of states in TiO_2 nanoparticles surrounded with aqueous electrolyte, *J. Solid State Electrochem.*, 2007, **11**, 647–653.

34 J. L. Movilla, G. Garcia-Belmonte, J. Bisquert and J. Planelles, Calculation of the electronic density of states induced by impurities in TiO_2 quantum dots, *Phys. Rev. B: Condens. Matter Mater. Phys.*, 2005, **72**, 153313.

35 B. O'Regan and J. R. Durrant, Calculation of Activation Energies for Transport and Recombination in Mesoporous TiO_2/Dye/Electrolyte Films-Taking into Account Surface Charge Shifts with Temperature, *J. Phys. Chem. B*, 2006, **110**, 8544–8547.

36 L. Feng, J. James Robert, M. Nripan and W. Qing, Evolution of Charge Collection/Separation Efficiencies in Dye-Sensitized Solar Cells Upon Aging: A Case Study, *J. Electrochem. Soc.*, 2011, **158**, B1158–B1163.

37 A. Listorti, C. Creager, P. Sommeling, J. Kroon, E. Palomares, A. Fornelli, B. Breen, P. R. F. Barnes, J. R. Durrant, C. Law and B. O'Regan, The mechanism behind the beneficial effect of light soaking on injection efficiency and photocurrent in dye sensitized solar cells, *Energy Environ. Sci.*, 2011, **4**, 3494–3501.

38 E. M. Barea, J. Ortiz, F. J. Payá, F. Fernández-Lázaro, F. Fabregat-Santiago, A. Sastre-Santos and J. Bisquert, Energetic factors governing injection, regeneration and recombination in dye solar cells with phthalocyanine sensitizers, *Energy Environ. Sci.*, 2010, **3**, 1985–1994.

39 E. M. Barea, C. Zafer, B. Gultekin, B. Aydin, S. Koyuncu, S. Icli, F. F. Santiago and J. Bisquert, Quantification of the Effects of Recombination and Injection in the Performance of Dye-Sensitized Solar Cells Based on N-Substituted Carbazole Dyes, *J. Phys. Chem. C*, 2010, **114**, 19840–19848.

40 R. Memming, *Semiconductor Electrochemistry*, Wiley-VCH, Weinheim, 2001.

